Voltage Weak DC Distribution Grids

Hailu, Tsegay; Mackay, Laurens; Ramirez-Elizondo, Laura M.; Ferreira, Jan A.

DOI
10.1080/15325008.2017.1319436

Publication date
2017

Document Version
Final published version

Published in
Electric Power Components and Systems

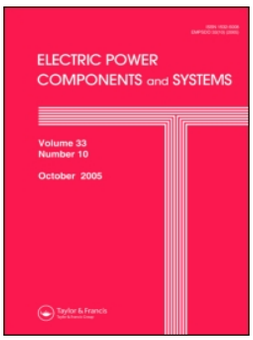

Taylor & Francis
Taylor & Francis Group

Electric Power Components and Systems

ISSN: 1532-5008 (Print) 1532-5016 (Online) Journal homepage: http://www.tandfonline.com/loi/uemp20

Voltage Weak DC Distribution Grids

Tsegay Gebremedhin Hailu, Laurens Mackay, Laura M. Ramirez-Elizondo & Jan A. Ferreira

To cite this article: Tsegay Gebremedhin Hailu, Laurens Mackay, Laura M. Ramirez-Elizondo & Jan A. Ferreira (2017) Voltage Weak DC Distribution Grids, Electric Power Components and Systems, 45:10, 1091-1105, DOI: 10.1080/15325008.2017.1319436

To link to this article: http://dx.doi.org/10.1080/15325008.2017.1319436

Published online: 28 Jul 2017.

Electric Power Components and Systems, 45(10):1091–1105, 2017

Tsegay Gebremedhin Hailu, Laurens Mackay, Laura M. Ramirez-Elizondo, and Jan A. Ferreira
ISSN: 1532-5008 print / 1532-5016 online
DOI: 10.1080/15325008.2017.1319436

Voltage Weak DC Distribution Grids

Tsegay Gebremedhin Hailu, Laurens Mackay,
Laura M. Ramirez-Elizondo, and Jan A. Ferreira
DC Systems, Energy Conversion & Storage (DCE&S), Delft University of Technology, Delft, Netherlands

CONTENTS

Abstract—This paper describes the behavior of voltage weak DC distribution systems. These systems have relatively small system capacitance. The size of system capacitance, which stores energy, has a considerable effect on the value of fault currents, control complexity, and system reliability. A number of potential definitions of voltage weak DC distribution systems are proposed. These definitions address the main characteristics of voltage weak systems. A small signal model of a general voltage weak DC distribution system is developed in order to observe sufficient conditions for system stability. This is achieved by analyzing the dominant poles. The source converters are modeled as droop-controlled current sources in parallel with their respective terminal capacitors. As constant power loads have incremental negative impedances, which affect the system stability, especially, in voltage weak system, ideal constant power loads with their terminal capacitors are included in the small signal model. A three-node voltage weak DC distribution grid is analyzed, as a case study, by implementing the developed small signal model. The effects on system stability by the values of system capacitance, cable inductance, and cable resistance are investigated using dominant pole placement. Likewise, the influence of proportional-integral regulators and droop coefficients of source converters on the stability of the system is examined. Finally, the three node DC distribution grid is developed in MATLAB/Simulink in order to demonstrate the influence of small capacitance on system stability. Moreover, effect of the rate of change of constant power loads on the system stability is simulated. These results are further compared and verified on a voltage weak DC experimental test bench with a 350 VDC bus voltage.

Keywords: voltage weak, DC distribution, system stability, rate of change of load power, dominant poles

Received 6 November 2016; accepted 5 April 2017

Address correspondence to Tsegay Gebremedhin Hailu, Delft University of Technology, Delft 2600 AA, Netherlands. E-mail: tsegazeabg@gmail.com
Color versions of one or more of the figures in the article can be found online at www.tandfonline.com/uemp.

1. INTRODUCTION

DC distribution grids and microgrids are currently challenging the conventional, bulky AC grid. Recently, application-based research has focused on the development of DC microgrids. These developments include areas such as data centers, naval ships, telecom systems, rural areas, and street lighting [1–5]. The research of DC grids or microgrids on the distribution level has gained momentum in connection with the increased utilization of renewable energy sources. All the research thus far has been based on arguments such as efficiency gain, control simplicity, and the overall decrease in the quantity of required converters and/or conversion

	Centralized	Decentralized	Distributed	Hybrid Distributed
Communication	Yes	No	Yes	No
Voltage regulation: precision	High	Intermediate	Intermediate	Low
Expandability	Low	High	High	High
Load sharing	Intermediate	Inaccurate	Precise	Inaccurate
Optimality	High	Impossible	Low	Low
Reliability	Low	High	Intermediate	High
Publications	[12]	[13]	[13, 14]	[15, 16]

TABLE 1. Comparison of power balancing strategies.

stages [6]. Although these arguments are perhaps the driving force behind application-based DC microgrid research, the main gain of DC grids over the conventional AC grid is the overall decrease in required copper in conducting lines at the expense of higher DC distribution voltages.

It can be noted that most DC microgrid research is centered on mimicking the behavior of the AC grid. This research is mainly focused on power balancing strategies, supervisory hierarchical control, and optimal power flow analysis [7]. Recently, research has been shifting the focus on exploring different system behaviors, system stability analysis, and dynamics [8].

Current-sharing control techniques of conventional DC microgrids are generally classified into four categories. These are centralized, decentralized, distributed, and hybrid distributed. Table 1 shows a compiled comparison of the power balancing strategies implemented in DC microgrids [7]. Centralized load sharing techniques require a dedicated central controller with a high degree of communication. The controller provides set points for each source by evaluating information that it receives from all sources. Although the load sharing is accurate, a loss in communication can lead to system failure.

Distributed control uses non-time critical and low-degree communication. Participating sources exchange information among each other. Each source gathers information, such as current and terminal voltages of other participating sources. Using an adaptive droop control algorithm, each source updates its set points. With distributed control, a high accuracy of voltage regulation and proportional power sharing can be achieved. The main advantage of this control technique is that a communication failure in one source does not necessarily lead to system failure. Power-based control of DC distribution systems, that uses non-time critical communication for sharing information regarding available stored energy or expected loads, has been investigated [9]. A weakly coupled DC microgrid design approach is presented in [10]. This design approach addresses estimating power set points for coupling converters connected to the bulk grid. It also demonstrates a power setting method for optimal storage utilization.

In a decentralized load sharing technique, there is no communication among participating sources. Load sharing algorithms are implemented in individual converters and are highly affected by the impedance of interconnection cables [11]. Voltage and power sharing accuracy is generally low. Hybrid distributed load sharing technique uses the system voltage as a de facto communication signal. This is nominally referred to as DC Bus Signaling (DBS). As a result, the overall reliability is high; however, voltage accuracy is low in hybrid distributed load sharing.

Generally, all the conventional current sharing control techniques can be implemented via a hierarchical, four-level control strategy [7]. These are inner, primary, secondary, and tertiary control. The inner controls are often voltage and current control techniques that are used to regulate the module's respective output values. Primary controls deal with droop control of DC sources like PV, battery, AC/DC converters and wind generators in DC microgrid. The secondary control ensures the electrical values (voltages and currents) in microgrids remain within a predefined range. It may, therefore, require communication between different modules and/or a central controller. The tertiary control handles power flow among different microgrids. Different implementation methods of these control levels (especially for the primary and secondary) have been the the subject of recent research [17].

The steady-state based control and power sharing techniques of DC microgrids are well studied. The stability analysis of microgrid systems is limited to either small microgrids [18] or large microgrids [13]. Small DC microgrid contains a single source and one/multiple identical loads. Usually, a detailed model of the system elements, which include the source, loads, and interconnecting cable, can be achieved. Therefore, the effect of each element on the system stability can be accurately examined. The source used in the modeling and analysis is the commonly known DC/DC converters such as buck, boost, or buck-boost topology.

Mostly, constant power loads are used in small DC microgrid for modeling and analysis. This is mainly due the fact that they introduce a negative incremental impedance during system disturbance. However, as the number of sources and loads increases, the system modeling and analysis become more complex and therefore, due to scalability limitation, no conclusions can be drawn for a large DC microgrid.

Therefore, to reduce the complexity of modeling and analysis, sources and loads are usually modeled as ideal in large microgrids. Large microgrids, in definition, include a number of different sources and different loads connected in certain architectures. The effects of cable inductance, cable resistance, and constant power loads on the system stability are studied in these types of microgrids. For instance, a very systematic mathematical analysis is implemented to investigate the effects of cable inductance and resistance on system stability [19]. However, the assumption made on source modeling, that converters have infinite bandwidth, makes the analysis to be impractical. The nature of power electronic converters with limited control bandwidth, and digital and/or analog processing time are mostly neglected. These have a profound influence on the value of system capacitance. This system capacitance value determines voltage dips, rises, or oscillation in the event of a load change or disturbance. Moreover, the use of high value system capacitance in the experiment contradicts the assumption made on source modeling in [19]. The effect of cable inductance and resistance for a cluster of microgrids is examined, and the eigenvalues are extracted from MATLAB [20]. Moreover, the use of large value capacitors, in the experiments provided in these papers, contradicts the assumptions made in the analysis.

Regardless of whether the microgrid is the small or large system, their system behavior is confined to limitations of inertia-full AC microgrids. The high inertia is obtained by adding higher value capacitors. This approach ensures the system behaves as "Voltage Stiff." The approach is mainly advantageous not only for easy control implementation but also for using the control methods already developed for AC grids [21]. However, the use of large system capacitance leads to a challenging situation of fault detection, isolation, and protection co-ordination in DC microgrids. The currently available AC circuit breakers are used in DC microgrids as the system inertia is relatively high. However, the unavailability of zero-crossing current during a DC fault creates a continuous arcing and longer time is required for arc quenching [22].

This paper proposes Voltage Weak Dc Distribution system (VWDD). The VWDD system utilizes small system capacitance, which leads to an overall low system inertia. However, the use of small capacitance in DC distribution makes the system more prone to system disturbance such as loads changes. Section 2 discusses different approaches to define voltage weak DC distribution. Section 3 presents small signal modeling of a voltage weak DC distribution grid. Section 4 shows a case study for a three-node DC distribution grid. The influences of cable parameters, terminal capacitors, and proportional-integrator (PI) values of converters on the system stability are presented. By observing the dominant pole placements, different system parameters are evaluated for sufficient stability conditions. Sections 5 and 6 demonstrate these concepts on simulation and an experimental setup respectively, and solutions to mitigate effects of the low inertia are shown. Finally, a conclusion is provided.

2. VOLTAGE WEAK DC DISTRIBUTION SYSTEMS: DEFINITION

In DC systems, inertia is mainly defined by the energy stored in the passive components (capacitors and inductors). The value of capacitance in the system mainly determines the value of the stored inertia. Therefore, systems with large inertia are defined as voltage stiff and systems with small inertia are defined as voltage weak. In converter-dominated DC grids, ideally fast controlled converters can eliminate the need for inertia in DC systems [19]. However, the practical implementation of such a control method, especially in high power converters is very unlikely, at least at this time [23].

VWDD systems have small system capacitance. This implies that they are characterized by low inertia. Systems with low inertia have a low prospective short circuit current. Therefore, voltage weak systems can be defined either from the perspective of inertia or from the perspective prospective short circuit currents. From the former perspective, as most DC distribution grids are converter dominated, voltage weak DC distribution grids can be defined using the converter inertia. The time constants of converters with respect to energy stored in their respective terminal capacitors can be estimated and standardized. For a modular DC distribution grid, the time constant of the modular system can be estimated by acquiring the complete system capacitance. From the latter perspective, the short circuit current to a rated protection device current ratio of each branch in a VWDD system can be defined for the protection device to work properly. This approach, however, requires fast signal measurement.

Therefore, in general, VWDD has three main characteristics. It has low capacitance and low short circuit current. It also requires the implementation of high-bandwidth converter for the system to properly function after a DC fault. However, in order to define the capacitance value, three different definitions are presented as potential approaches. These are converter based, system based and low fault current

based. These approaches are briefly discussed in the next subsections.

2.1. Converter-based Definition

DC distribution grids are expected to be dominated by converters. Sources and loads are connected to the DC distribution grid by power electronics converters. Interconnection among DC distribution grids is currently being implemented by DC/DC converters. Therefore, the output capacitance of these converters play a major role in DC distribution grid system stability.

Defining the inertia of the individual converters provides a general selection criteria of capacitance for converter with a given power in VWDD grid. The size of effective inertia provided by the terminal capacitors of converter is dependent on not only the capacitance value but also the minimum system voltage.

The time for the terminal capacitors of converters to reach the minimum voltage ($V_{\min}$) from the nominal voltage (V_{Nom}) while the rated power of the converters (P_{rated}) is drawn from the terminal capacitors can be easily estimated. If minimum voltage is α % of the nominal voltage and C is the capacitance of a converter, the time constant, τ, is given by Eq. (1). The derivation is presented in Appendix A. This time constant provides critical time information for determining the converter control bandwidth. To avoid system collapse, the time constant of the converter's controller has to be faster than τ. This definition is dependent on individual converters. This can cause stability issues if the system is not well defined

$$\tau = \frac{(1-\alpha^2)CV_{\text{Nom}}^2}{2P_{\text{rated}}} \tag{1}$$

2.2. System-based Definition

Another way of defining a VWDD is using the whole system capacitance to calculate the average time constant of the DC distribution grid. The average time constant τ_{ave} is expressed as the average of individual converters' time constants. Equation (2) shows the estimated τ_{ave} for an allowable voltage change, which is α % of the V_{Nom} for rated converter power P_{rated_n} and respective capacitance, C_n, of each converter. This approach uses the total energy stored in the system during the rated system power change and estimates averaged system time constant for N number of sources. The mathematical derivation of τ_{ave} is provided in Appendix B

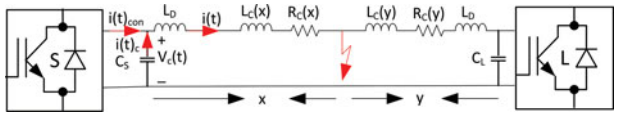

FIGURE 1. A source and load connection in DC distribution power system.

$$\tau_{\text{ave}} = \frac{\sum_{n=1}^{N} \frac{(1-\alpha^2)V_{\text{Nom}}^2 C_n}{2P_{\text{rated}_n}}}{N} \tag{2}$$

In a dynamic system, the estimated τ_{ave} varies with an addition or removal of converters in the network. This approach is mainly useful for a meshed and highly modular DC distribution system.

2.3. Low-Fault-Current-based Definition

VWDD has low fault current values during various short circuit conditions. However, the low fault current has to be estimated, to systematically define fault current limits for both individual converters and circuit breakers. The ratio of fault current at desired fault isolation time, τ, to the rated cable current (I_{ca}), can be easily estimated using network parameters. This ratio is here referred to as β. Figure 1 is a simple DC distribution grid featuring line impedances and decoupling inductances at the terminals of the converters. The decoupling inductance limits the rise of current and also filters high-frequency signals, either from disturbances or power line communication signals.

For a fault x km away from the converter, the fault current is shown in Eq. (3), with both the converter and cable initial currents at steady state, I_o. As the bandwidth of the converters is low, the current from the sources can be assumed to be constant in the first few μs. The peak current is dependent on the values of C and L, where L is the sum of decoupling inductance (L_D)and cable inductance ($L_C(x)$). Only the terminal capacitance can be predetermined. With the increase in cable length, the inductance increases and therefore, the minimum capacitance is estimated in order to ensure that the decoupling inductance achieves the maximum allowable fault current. β, the current ratio, can be estimated using Eq. (3) (Derivation in Appendix C);

$$i(t) = \frac{I_o e^{-\frac{t\left(\frac{\sqrt{C_s R^2 - 4L}}{\sqrt{C_s}} + R\right)}{2L}} \left(\sqrt{C_s R^2 - 4L}\left(e^{\frac{t\sqrt{C_s R^2 - 4L}}{\sqrt{C_s}L}} + 1\right) + \sqrt{C_s}R\left(e^{\frac{t\sqrt{C_s R^2 - 4L}}{\sqrt{C_s}L}} - 1\right)\right)}{2\sqrt{C_s R^2 - 4L}} \tag{3a}$$

$$\beta = \frac{i(\tau)}{I_{ca}} \tag{3b}$$

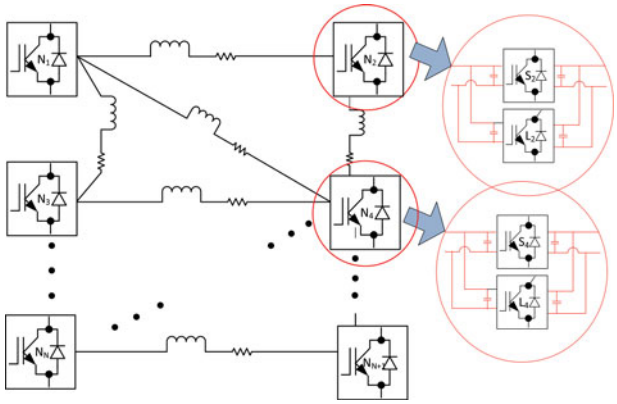

FIGURE 2. A generalized voltage weak DC distribution grid under investigation based on the concepts described in [19].

This peak current limiting approach is specifically important in ensuring converter isolation during a bolt fault. Therefore, this approach can be extended to be realized for all converters in a network.

3. DC DISTRIBUTION GRID ARCHITECTURE: MODELING

The architecture of a DC distribution grid is still an open research field to be investigated. Meshed DC distribution grids are believed to be an optimal solution. For a meshed DC distribution, the basic component is a modular subsystem as shown in Figure 2. These kinds of modular subsystems make the system stability analysis more practical. Depending on the value of system passive components as described in Section 2, the distribution system can be defined as weak or stiff.

In this section, a voltage weak DC distribution architecture is modeled. Each node has a source and a load as shown in Figure 2. The source is modeled as voltage-controlled current sources in parallel with a terminal capacitor. Its terminal current is regulated via a PI controller that receives the necessary reference value from a voltage droop set point. The following subsections present the small signal modeling of sources, loads, interconnecting cables, and the complete DC distribution grid.

3.1. Source Modeling

The source and its control are modeled as shown in Figure 3. Droop control is implemented for the secondary control, with the inner voltage and current control simplified by a voltage-controlled PI regulator as approximated in [24]. First-order filters, as an approximated replacement for the PI current controls, are not included in the modeling. In a voltage weak DC

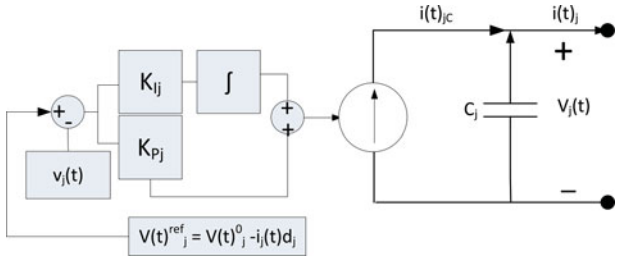

FIGURE 3. Modeling of the sources.

distribution grid, high-frequency power signals are a possibility and filtering them would limit the system control dynamics. The analysis includes all power signal frequencies below the voltage PI controller cutoff frequency. All relevant current and voltage equations for the jth node include the following:

$$i_{jc} = i_j + c_j \frac{dv_j}{dt} \tag{4a}$$

$$i_{jc} = i_{jco} + k_{Pj}\left(v_j^{ref} - v_j\right) + k_{Ij}\int\left(v_j^{ref} - v_j\right)dt \tag{4b}$$

$$v_j^{ref} = v_j^o - d_j i_j \tag{4c}$$

where v_j, i_{jc}, v_j^{ref}, v_j^o, c_j, d_j, i_{jco}, k_{Pj}, and k_{Ij} are terminal voltage, capacitor current, voltage reference, nominal voltage, terminal capacitor, droop gain, initial current of the capacitor, and proportional-integral values of PI voltage controller at terminal j, respectively.

Linearizing Eq. (4), the small signal equations of the source model in matrix form, both in time and frequency domains are shown in Eq. (5):

$$\hat{\mathbf{i}}_c = \hat{\mathbf{i}} + \mathbf{C}\frac{d\hat{\mathbf{v}}}{dt} \tag{5a}$$

$$\hat{\mathbf{i}}_c = \mathbf{K}_p(\hat{\mathbf{v}}_{ref} - \hat{\mathbf{v}}) + \mathbf{K}_i\int(\hat{\mathbf{v}}_{ref} - \hat{\mathbf{v}})dt \tag{5b}$$

$$\hat{\mathbf{v}}_{ref} = -\mathbf{D}\hat{\mathbf{i}} \tag{5c}$$

$$\hat{\mathbf{i}}_c(s) = \hat{\mathbf{i}}(s) + s\mathbf{C}\hat{\mathbf{v}}(s) \tag{5d}$$

$$\hat{\mathbf{i}}_c(s) = \mathbf{K}_p(\hat{\mathbf{v}}_{ref}(s) - \hat{\mathbf{v}}(s)) + \frac{\mathbf{K}_i}{s}(\hat{\mathbf{v}}_{ref}(s) - \hat{\mathbf{v}}(s)) \tag{5e}$$

$$\hat{\mathbf{v}}_{ref}(s) = -\mathbf{D}\hat{\mathbf{i}}(s) \tag{5f}$$

where $\hat{\mathbf{v}}$, $\hat{\mathbf{i}}$, $\hat{\mathbf{i}}_c$, and $\hat{\mathbf{v}}_{ref}$ are diagonal matrices, $n \times 1$, of voltages, currents, capacitor currents, and voltage references, respectively. $\mathbf{C}$, $\mathbf{K}_p$, $\mathbf{K}_i$, and $\mathbf{D}$ are diagonal matrices $n \times n$ of terminal capacitors, proportional, and integral values of PI controller, and droop gains, respectively. n represents the number of nodes.

3.2. Line Modeling

By applying Kirchhoff law for the network represented in Figure 2, the voltage and current equations across the connection point between two nodes, j and k, are:

$$v_{jk} = l_{jk}\frac{di_{jk}}{dt} + r_{jk}i_{jk} \tag{6a}$$

$$v_{jk} = v_j - v_k \tag{6b}$$

$$i_j = i_{Lj} + i_{jk} \tag{6c}$$

where v_{jk}, i_{jk}, l_{jk}, and r_{jk} are the branch voltage, current, inductance, and resistance, respectively. i_{Lj} is the load current at terminal j.

Linearizing Eq. (6), the small signal equations of the line model in matrix form for the whole system, for both time and frequency domains are shown in Eq. (7):

$$\hat{\mathbf{v}}_B = \mathbf{L}\frac{d\hat{\mathbf{i}}_B}{dt} + \mathbf{R}\hat{\mathbf{i}}_B \tag{7a}$$

$$\hat{\mathbf{v}}_B = \mathbf{M}\hat{\mathbf{v}} \tag{7b}$$

$$\hat{\mathbf{i}} = \hat{\mathbf{i}}_L + \mathbf{M}^T\hat{\mathbf{i}}_B \tag{7c}$$

$$\hat{\mathbf{v}}_B(s) = s\mathbf{L}\hat{\mathbf{i}_B}(s) + \mathbf{R}\hat{\mathbf{i}}_B(s) \tag{7d}$$

$$\hat{\mathbf{v}}_B(s) = \mathbf{M}\hat{\mathbf{v}}(s) \tag{7e}$$

$$\hat{\mathbf{i}}(s) = \hat{\mathbf{i}}_L + \mathbf{M}^T\hat{\mathbf{i}}_B(s) \tag{7f}$$

where $\hat{\mathbf{v}_B}$, $\hat{\mathbf{i}}_B$, and $\hat{\mathbf{i}}_L$ are column vectors of branch voltages, branch currents, and load currents, respectively. $\mathbf{L}$ and $\mathbf{R}$ are the diagonal matrices of cable inductance and resistance, respectively. $\mathbf{M}$ is an $n \times m$ matrix of 1, 0, or -1 that represents any connection among different nodes and current directions, where n is the number of nodes and m is the number of interconnecting cables.

3.3. Load Modeling

The loads are modeled either as ideal constant power loads (CPL) [8] or resistive loads. Linearized small signal model of CPL is expressed as current sink (u_j) in parallel with a negative incremental conductance (g_j). This model is shown in Eq. (8b) [19]. The resistance is modeled as shown in Eq. (8c):

$$i_{Lj} = -g_j v_j + u_j \tag{8a}$$

Constant power load:

$$g_{jP} = \frac{p_j}{v_j^2} \quad u_{jP} = 2\frac{p_j}{v_j} \tag{8b}$$

Resistive load:

$$g_{jR} = -\frac{1}{R_j} \quad u_{jR} = 0 \tag{8c}$$

where p_j is the load power at the jth node, v_j is the operating voltage at the jth node, and R_j is the load resistance at the jth node.

The conductance, G_j, is the sum of G_{jP} and G_{jR} as described in Eq. (9), where M_{CPL} and M_R are diagonal matrices of $n \times n$ with values of 1 and 0 to show whether there is a constant power load or a resistive load at each node, respectively

$$G_j = G_{\mathrm{jP}}M_{\mathrm{CPL}} + G_{\mathrm{jR}}M_{\mathrm{R}} \tag{9}$$

The linearized small signal of the loads in a matrix form in time and frequency domain is

$$\hat{\mathbf{i}}_l = -\mathbf{G}\hat{\mathbf{v}} + \hat{\mathbf{u}} \tag{10a}$$

$$\hat{\mathbf{i}}_l(s) = -\mathbf{G}\hat{\mathbf{v}}(s) + \hat{\mathbf{u}}(s) \tag{10b}$$

where $\hat{\mathbf{i}}_l$ and $\hat{\mathbf{u}}$ are a column matrix of load current and current sink, respectively. $\mathbf{G}$ is the diagonal matrix of load conductances.

4. CASE STUDY: SMALL SIGNAL ANALYSIS: THREE NODE GRID

In the small signal analysis of the system, the input is the change in the constant current of the CPL or a small change in resistive load ($\hat{\mathbf{u}}$). The output is the terminal voltage of the sources that is voltage across the capacitors ($\hat{\mathbf{v}}$). Using the linearized and Laplace transformed small signal equations from (5) to (10), the Multiple-Input Multiple Output (MIMO) transfer function is presented in Eq. (11):

$$\frac{\hat{\mathbf{v}}(s)}{\hat{\mathbf{u}}(s)} = (\mathbf{C}s^2 + \mathbf{K}_{\mathrm{p}}s + \mathbf{K}_{\mathrm{i}} + (((\mathbf{K}_{\mathrm{p}}\mathbf{D} + \mathbf{I})s + \mathbf{K}_{\mathrm{i}}\mathbf{D}) \times (\mathbf{M}^T(\mathbf{L}s + \mathbf{R})^{-1}\mathbf{M} - \mathbf{G})))^{-1}((-\mathbf{K}_{\mathrm{p}}\mathbf{D} - \mathbf{I})s - \mathbf{K}_{\mathrm{i}}\mathbf{D}) \tag{11}$$

The main objective of this paper is primarily to demonstrate the effect of passive components, droop coefficients, and PI values on the system stability. For this, the MIMO is simplified into a Single Input Multiple Output (SIMO) equation. Only one load, at node x, changes at a given time, t, and the analysis is implemented using the following condition:

$$\hat{u}(t)_j = \begin{cases} \hat{u}(t)_x, & \text{if } j = x \\ 0, & \text{if } j \neq x \end{cases} \tag{12}$$

For the three node system shown in Figure 4, a change in node 1 is considered. The voltage stability is analyzed by observing the dominant pole movements of corresponding transfer functions. In the analysis, the values in Table 2 are used unless otherwise mentioned.

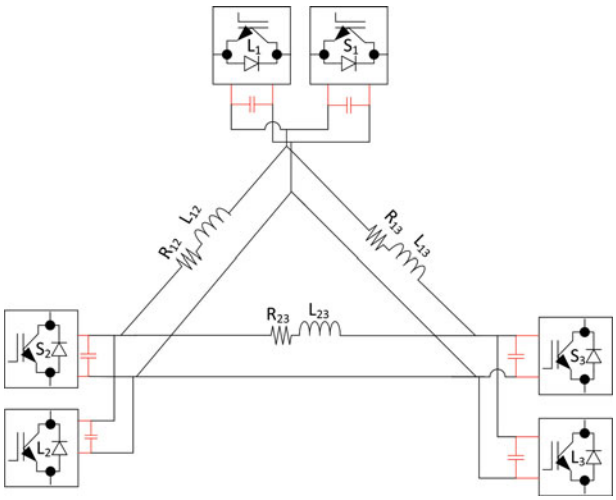

FIGURE 4. Three node voltage weak DC distribution system.

4.1. Effect of Capacitance

The effect of capacitance on the system stability is examined by the location of dominant poles of the transfer function by assuming a change in node one. Figure 5 presents the movement of the dominant poles when the terminal capacitances at each node are varied from 1 µF to 10 mF for three different values of cable inductances in all branches. The cable inductance varies depending on the line length and is increased to analyze the stability. Increasing both the terminal capacitance and line inductances lowers the oscillation frequency. This can be easily controlled by the voltage controller or an additional current controller. However, with small capacitance, the oscillations become high in frequency, which leads to need of a higher bandwidth current or voltage controller. Additionally, an external high bandwidth low power converter can be used to control the high-frequency oscillations, which is not the subject of this paper.

Variables	Values
K_P	0.9
K_I	400
D	0.01–0.4
C	1 μF to 10 mF
L	14 μH to 10 mH
R	1 mΩ to 0.2 Ω
M	$\begin{bmatrix} 1 & -1 & 0 \\ 0 & 1 & -1 \\ 1 & 0 & -1 \end{bmatrix}$
P	10 kW
RL	12.25 Ω
V	+350 VDC

TABLE 2. Value of system and component parameters used in the analysis.

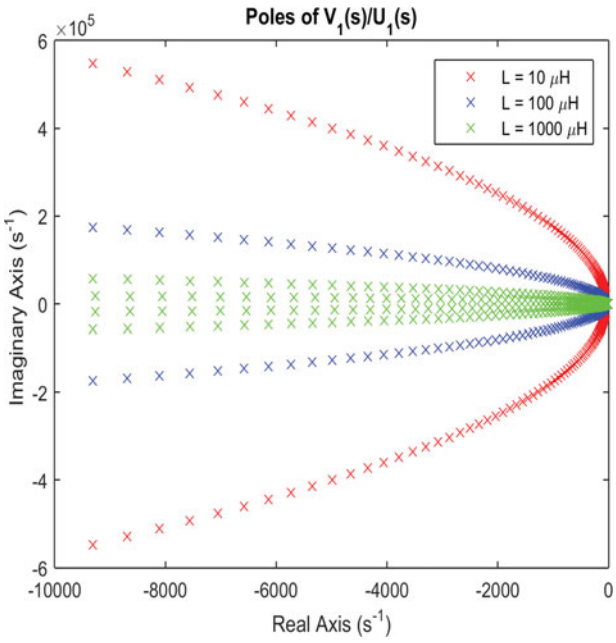

FIGURE 5. Dominant poles for node one for $\frac{v(s)_1}{u(s)_1}$. Three values of inductance, 10 µH, 100 µH, and 1 mH are used as the capacitance varies from 1 µF to 1 mF.

4.2. Effect of Droop

Increasing droop coefficients from 0.01 Ω to 10 Ω shifts the poles from a higher oscillation level (imaginary axis) to a lower region, as shown in Figure 6. When the capacitance is 1000 µF, the poles are at a less oscillatory region, as shown in Figure 6(b), compared to a 10 µF shown in Figure 6(a). For droop coefficients greater than 0.5 Ω, the poles move to the right half plane, which represents the unstable region. This limits the system droop values that can be used for a specified system.

4.3. Effect of Controller Proportional Value

By varying the proportional value of the voltage controller and terminal capacitors of the sources, the placement of dominant poles of the voltage transfer function for a change in load at node one is depicted in Figure 7. Decreasing the proportional values moves the poles to a more oscillatory region and also increases the voltage overshoot at node one. Increasing the capacitance value of the terminal capacitors leads to a further increase of the system stability, as can be inferred in Figure 7(b). Therefore, the decrease in system capacitance

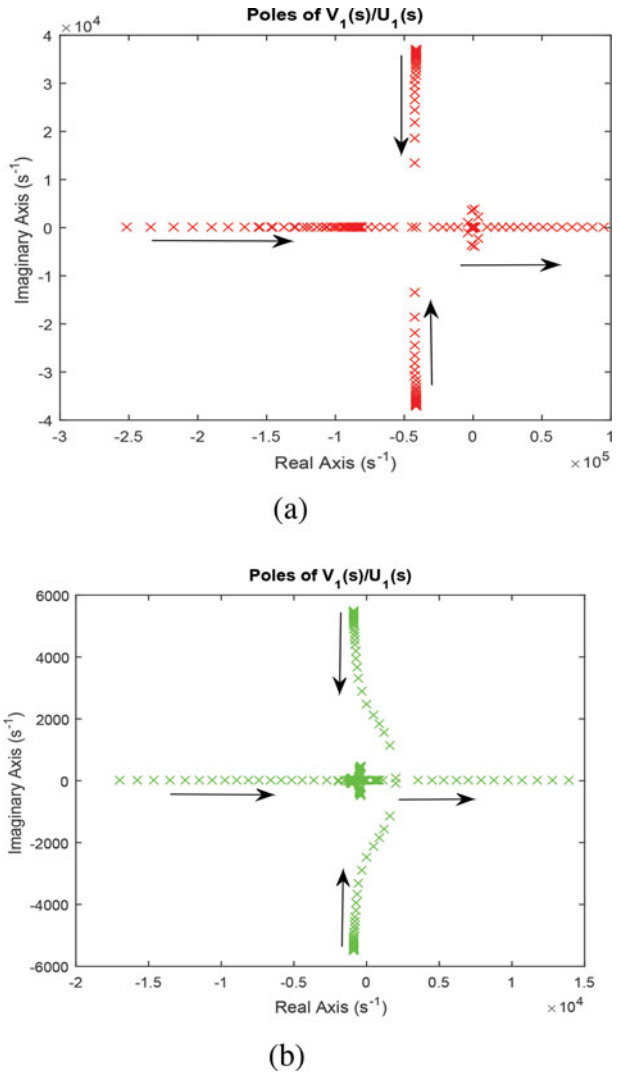

FIGURE 6. Placement of dominant poles as droop varies from 0.02 to 10 Ω. (a) Terminal capacitance, 10 μF and inductance, 100 μH. (b) Terminal capacitance, 1000 μF and inductance, 100 μH.

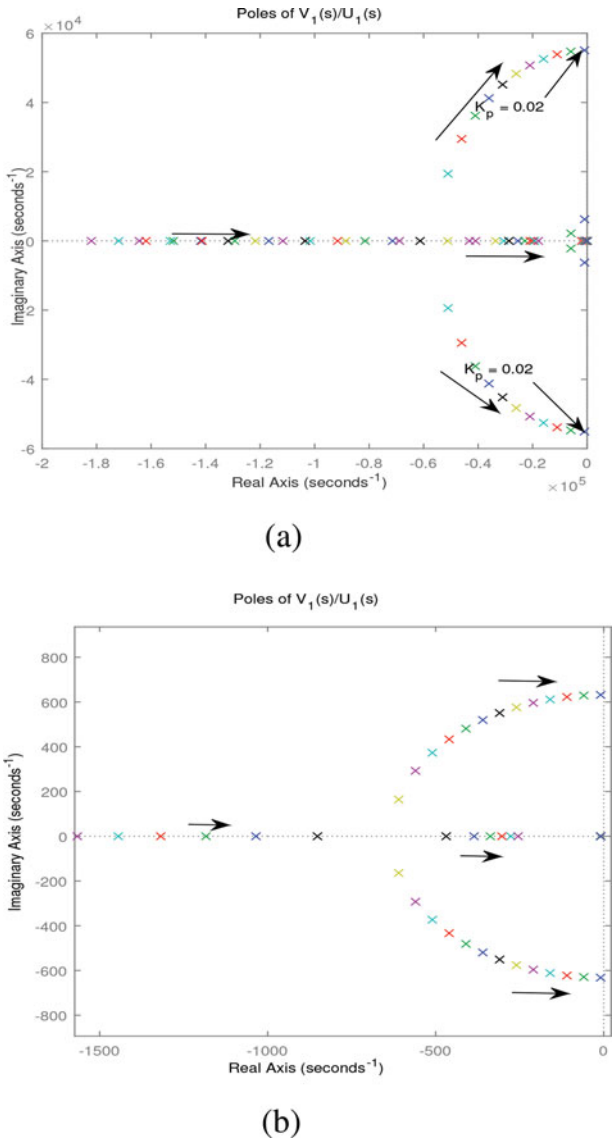

FIGURE 7. Placement of dominant poles as the proportional controller value varies from 2 to 0.01. (a) Terminal capacitance, 10 μF and inductance, 100 μH. (b) Terminal capacitance, 1000 μF and inductance, 100 μH.

and the increase in the proportional value lead to the system instability in the event of system disturbance as shown in Figures 7(a) and 7(b).

4.4. Effect of Controller Integral Value

Keeping the line inductances, resistances, and droop values constant, the value of integral in the voltage controller is varied to see its effect on the system stability for different values of the terminal capacitors of the converters. At low value of converter terminal capacitance, increasing the integral values increases the system oscillation. In the case of higher values of system capacitance, the oscillating dominant poles move to less oscillatory regions. However, the non-oscillating dominant poles move to the left, which decreases damping time as shown in Figures 8(a) and 8(b).

4.5. Effect of Line Resistance and Inductance

The effect of the line resistances and inductances is shown in Figure 9. Increasing the line inductances and resistances proportionally moves the non-oscillatory dominant poles to the left. Moreover, the oscillatory and overshooting dominant poles move to a lesser oscillatory values. By increasing the capacitance for the same value of line inductance

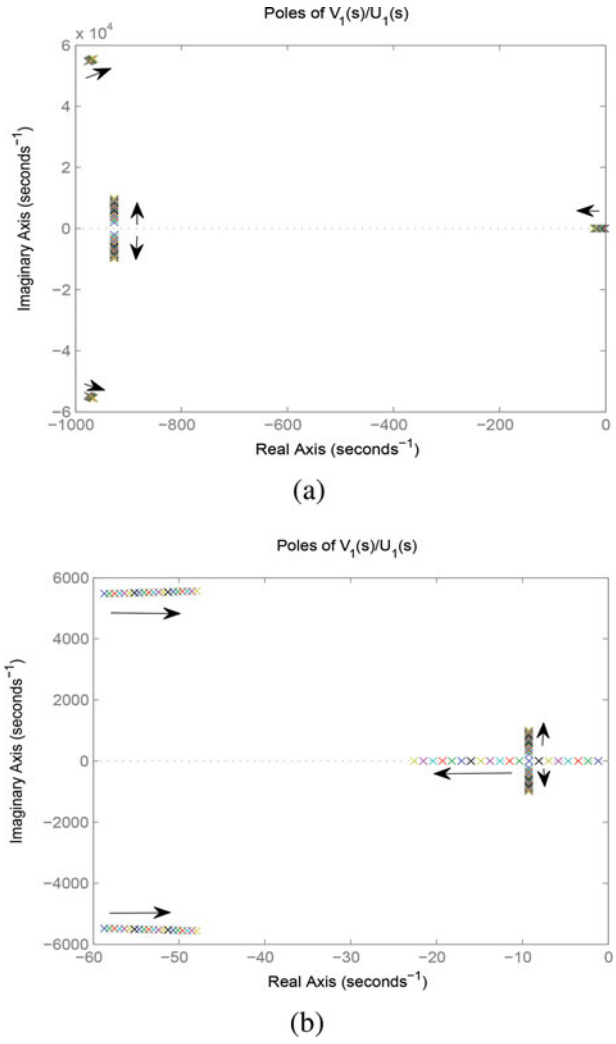

FIGURE 8. Placement of dominant poles as integral value varies from 50 to 1000. Droop value is set to 0.01 Ω and line resistance to 10 mΩ. (a) Terminal capacitance, 10 μF and inductance, 100 μH. (b) Terminal capacitance, 1 mF and inductance, 100 μH.

and resistance, the level of oscillation decreases, as shown in Figures 9(a) and 9(b).

5. THREE NODE VOLTAGE WEAK DC DISTRIBUTION GRID: SIMULATION

A voltage weak DC distribution grid with three sources and loads is simulated in MATLAB/Simulink to demonstrate the effect of system capacitance on system stability. The sources are modeled as a voltage controlled current sources as approximated in [24]. The current controllers of the sources are approximated with first-order filters. The voltage controllers are PI regulator. The voltage reference of each source is set by droop control where the reference is calculated by subtracting the product of measured current and the droop coefficient from the nominal voltage.

The loads are modeled as ideal constant power loads. Developing a very fast controller that addresses the voltage weak system is a more advantageous solution but currently impractical. In this paper, the DC grid voltage is controlled indirectly by limiting the rate of change of loads during black-start conditions. By implementing different rates of change for the loads, the stability of this three-node DC low capacitance distribution grid is examined.

From Figures 6–9, for the three node case study, it is demonstrated that a small step load change in a voltage weak grid could lead to an oscillation or overshoot or voltage dip depending on the system parameters. In a working

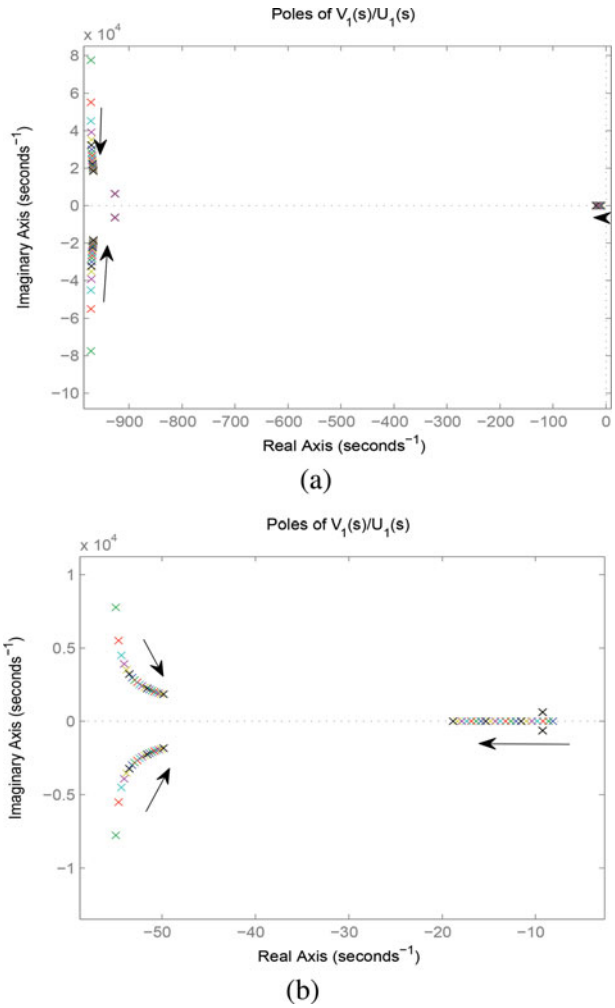

FIGURE 9. Placement of dominant poles as line resistance and inductance are proportionally multiplied by the same factor that varies from 1 to 100. (a) System capacitance, 10 μF. (b) Terminal capacitance, 1 mF.

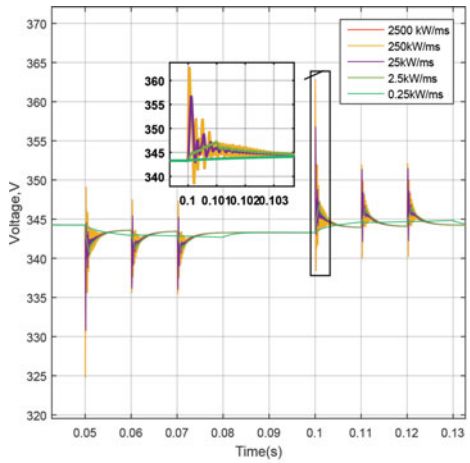

(a)

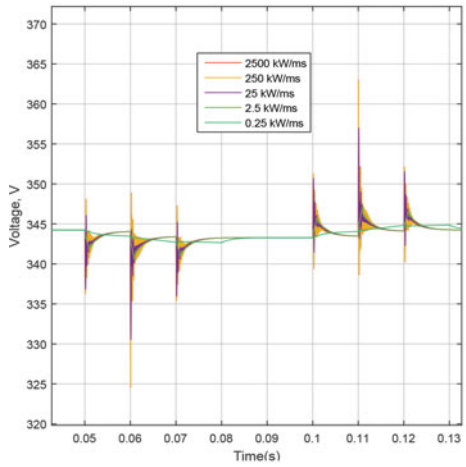

(b)

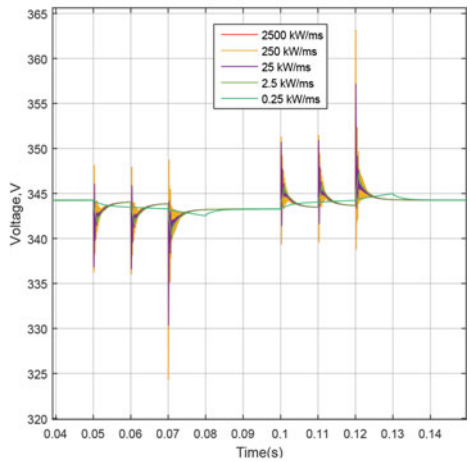

(c)

FIGURE 10. Effect of rate of change of loads on terminal voltages of a voltage weak DC distribution system. Load changes are applied to each node at different time intervals. (a) Voltage behavior of the first node. (b) Voltage behavior of the second node. (c) Voltage behavior of the third node.

distribution grid, the disturbances are mainly characterized by load changes, most often, turning on and off. In these instances, if the rate of change of loads is faster than the rate of change of source, the system voltage collapses. Moreover, loads are designed with no standard rate of change during these conditions.

Some loads may have a relatively faster switching time than others. Therefore, in a voltage weak DC distribution grid, a slower rate is recommended to avoid a low voltage dip in the system if not voltage collapse. With the values of system parameters depicted in Table 3 and a DC distribution grid shown in Figure 4, the system voltage dynamics is observed for different rates of change of loads.

For a voltage weak DC distribution grid, a slow load change allows the system sources to react before the system fails. In the case of the simulated system, decreasing the rate of change of loads decreases the voltage dips when loads are added, and voltage rises in cases when the loads are disconnected. Figure 10 features voltage dips and rises at node one when the three loads are turning on/off at different intervals. By decreasing the rate of change of loads from 2500 kW/ms to 0.25 kW/ms, the voltage dip or rise substantially decreases. This rate of change of loads can be implemented in most loads with relative ease.

With some knowledge of the system capacitance and parameters of the sources in the system, the rate of change of loads can be standardized. For instance, one easy approach is to simply specify that every load comes with some fixed capacitance in relation to its power size. This approach leads to using the converter-based definition described in Section 2. Therefore, the capacitance value determines the rate of change of the load during turning on/off conditions.

6. EXPERIMENTAL RESULTS

A voltage weak DC microgrid demonstration is built as shown in Figure 11(a), with a 350 VDC bus and a configuration shown in Figure 11(b). The three converters are bidirectional

Variables	Values
K_P	0.9
K_I	400
D	0.2
C	1 µF
L	1 µH
R	1 mΩ
Power	5 kW each load
Voltage	+350 VDC

TABLE 3. Parameter values of the simulated system.

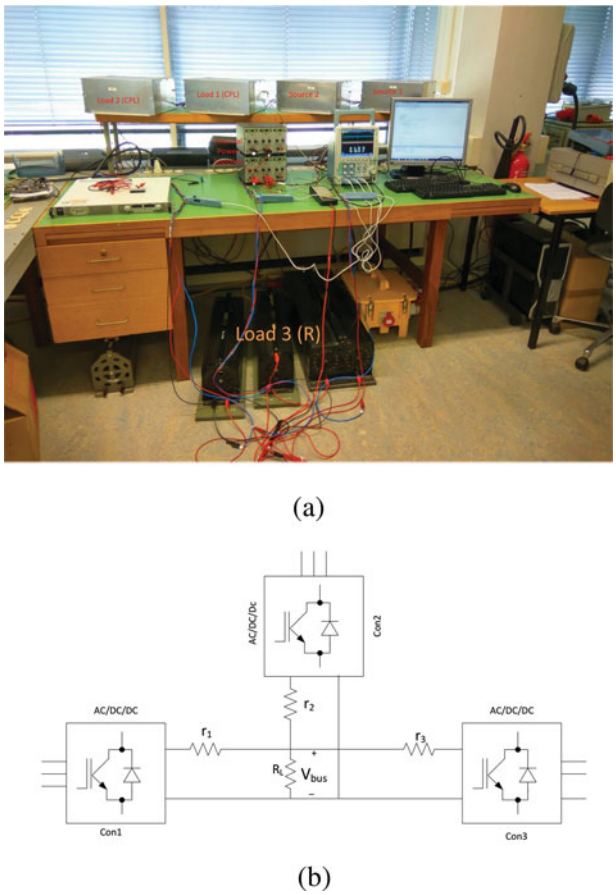

FIGURE 11. (a) Voltage weak DC microgrid experimental setup. (b) Laboratory setup system configuration.

AC/DC converters. These converters consist of two stages of conversion process, which is a combination of a voltage source AC/DC converter and a full bridge DC/DC converter. The maximum current of the converters is 5 A. The two source converters (Con1 and Con2) are set to a droop coefficient of 6 and the third (Con3) is programmed to behave as a constant power load. The voltage and current PI controller values of the sources are $K_{vp} = 1$, $K_{vi} = 130$, $K_{ip} = 2.5$, and $K_{ii} = 13$, respectively. The DC side capacitor value of the converters is 3 µF. The load converter is programmed as constant power load with programmable rate of power change. The maximum rate of change of the constant power load is 5000 W s^{-1}.

For the first experiment, a 70 Ω resistive load is connected via a mechanical switch. Due to the small system capacitance and slow reaction of the source converters, a voltage dip occurs as shown in Figure 12(a) when the switch is turned on. The measured current waveforms of Con1 and Con2 are shown in Figures 12(b) and 12(c), respectively. However, there is no oscillation as the resistive load dumps it.

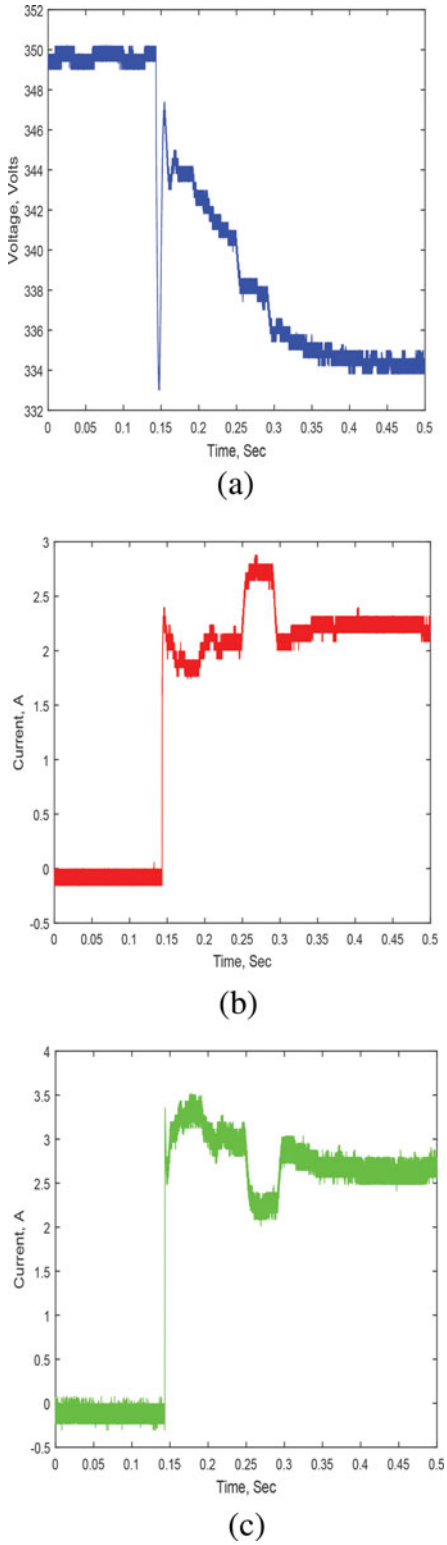

FIGURE 12. Effect of resistive load connection via a mechanical switch on the system dynamics. (a) System bus voltage. (b) Measured output current of Con1. (c) Measured output current of Con2.

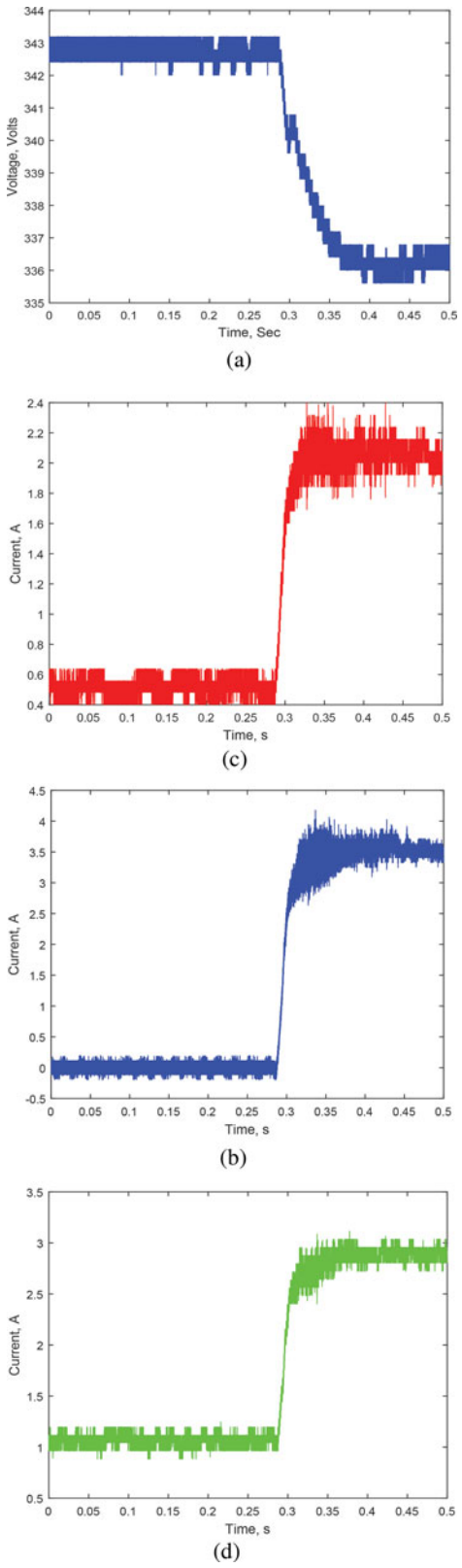

FIGURE 13. Measured system voltage and currents at 1000 W s^{-1} rate of change of the load. (a) Bus voltage. (b) Load Current. (c) Source one current. (d) Source two current.

In the second experiment, one of the converters is used as a constant power load, 1000 W, with rate of change of power 1000 W s^{-1}, while the other two converters are used as sources. The constant power load is switched on while a resistive load of 250 Ω is already connected to the bus. By making the load change slowly, the system voltage experiences small voltage dip. The bus voltage, load current, and source currents are shown in Figure 13. With a small system capacitance, the system dynamics can be altered by controlling the load's rate of change of power.

7. CONCLUSION

DC microgrids are currently being under the focus of intense research as a potential alternative to the ubiquitous AC grid. The research is mainly concentrated on small-scale application-based microgrids. Moreover, simulations and mathematical analysis also focus on small-scale applications.

In terms of system behavior, the small-scale applications imitate the current bulk AC grid. This is due to the fact that AC grid has large stored inertia. However, large system inertia in DC grid creates the main concern for system control, protection, and grounding. Designing DC grids to exhibit relatively high inertia leads to a requirement of large system capacitance, the alternative being to build higher rated system converters with fast controllers.

Large system capacitance leads to protection complexities. However, DC grid with less inertia exhibits low fault current. This helps in using low short-circuit current protection strategies and devices at the cost of control complexities. This paper introduces voltage weak DC distribution grid, which has low system inertia.

This paper proposes a voltage weak DC distribution as an alternative for a voltage stiff DC grid. Three ways of defining voltage weak DC distribution grid are provided. These definitions are based on system time constant, converter time constant, and low fault current based. The definitions provide a systematic approach in estimating the system inertia and developing a preliminary stability analysis of the DC distribution system.

Small signal modeling and analysis of voltage weak DC distribution system is provided. Effects of passive components such as terminal capacitor and cable inductance on system stability are investigated. Moreover, voltage control PI values and droop coefficients on system stability are addressed by observing the movement of dominant pole placement. The developed modeling and analysis approach can be used to assess sufficient conditions of stability of DC distribution grid given the parameters of the converters and interconnecting cables.

This paper also proposes a different approach to decrease the voltage dips and rises due to low system capacitance. The loads in the system are controllable and implement a variable rate of change of turning on/off to avoid system collapse. This, in general, constitutes a system smart. Simulations in MATLAB/Simulink are provided to demonstrate the effect of large signal changes, such as switching off/on of loads.

An experimental setup is also built to provide insight into the effect of system capacitance and rate of change of loads and how limiting the rate of change of loads provides system stability.

ORCID

Laurens Mackay http://orcid.org/0000-0002-4851-7426

REFERENCES

[1] Becker, D. J., and Sonnenberg, B. J., "DC microgrids in buildings and data centers," *International Telecommunication Energy Conference (INTELEC)*, 2011.

[2] Jin, Z., Sulligoi, G., Cuzner, R., Meng, L., Vasquez, J. C., and Guerrero, J. M., "Next-generation shipboard dc power system: Introduction smart grid and dc microgrid technologies into maritime electrical netowrks," *IEEE Electrif. Mag.*, Vol. 4, No. 2, pp. 45–57, June 2016.

[3] Johnson, M. A., and Smith, P. D., "Eco priority source dc micro-grids in telecom sites," *IEEE 1st International Conference on DC Microgrids (ICDCM)*, pp. 165–170, June 2015.

[4] Ibrahim, M., Chowdhury, S. A., Huda, M. N., and Khan, M. R., "A smart solution for solar dc nano grid integrated with prepaid billing and mobile application," *3rd International Conference on Electrical Engineering and Information Communication Technology (ICEEICT)*, pp. 1–6, September 2016.

[5] Rani, B. I., Ilango, G. S., and Nagamani, C., "Control strategy for power flow management in a pv system supplying dc loads," *IEEE Trans. Ind. Electron.*, Vol. 60, No. 8, pp. 3185–3194, August 2013.

[6] Nilsson, D., and Sannino, A., "Efficiency analysis of low- and medium-voltage dc distribution systems," *IEEE Power Engineering Society General Meeting*, Vol. 2. IEEE, pp. 2316–2322, 2004.

[7] Guerrero, J. M., Vasquez, J. C., Matas, J., de Vicuna, L. G., and Castilla, M., "Hierarchical control of droop-controlled AC and DC microgrids–A general approach toward standardization," *IEEE Trans. Ind. Electron.*, Vol. 58, No. 1, pp. 158–172, January 2011.

[8] Radwan, A. A. A., and Mohamed, Y. A. R. I., "Linear active stabilization of converter-dominated DC microgrids," *IEEE Trans. Smart Grid*, Vol. 3, pp. 203–216, 2012.

[9] Caldognetto, T., Tenti, P., and Brandao, D. I., "Power-based control of low-voltage microgrids," in *2014 IEEE Energy Conversion Congress Exposition* IEEE, pp. 4282–4289, September 2014.

[10] Hailu, T., Mackay, L., Ramirez-Elizondo, L., Gu, J., and Ferreira, J. A., "Weakly coupled DC grid for developing countries: Less is more," *AFRICON*. IEEE, pp. 1–5, September 2015.

[11] Haileselassie, T. M., and Uhlen, K., "Impact of dc line voltage drops on power flow of mtdc using droop control," *IEEE Trans. Power Syst.*, Vol. 27, No. 3, pp. 1441–1449, August 2012.

[12] Wang, B., Sechilariu, M., and Locment, F., "Intelligent DC microgrid with smart grid communications: Control strategy consideration and design," *IEEE Trans. Smart Grid*, Vol. 3, pp. 2148–2156, 2012.

[13] Anand, S., Fernandes, B. G., and Guerrero, J., "Distributed control to ensure proportional load sharing and improve voltage regulation in low-voltage DC microgrids," *IEEE Trans. Power Electron.*, Vol. 28, No. 4, pp. 1900–1913, April 2013.

[14] Qiu, W., and Liang, Z., "Practical design considerations of current sharing control for parallel VRM applications," *20th Annual IEEE Applied Power Electronics Conference Exposition (APEC'05).*, Vol. 1. IEEE, pp. 281–286, 2005.

[15] Zhang, L., Wu, T., Xing, Y., Sun, K., and Gurrero, J. M., "Power control of DC microgrid using DC bus signaling," *26th Annual IEEE Applied Power Electronics Conference Exposition*, IEEE, pp. 1926–1932, March 2011.

[16] Schonbergerschonberger, J., Duke, R., and Round, S., "DC-bus signaling: A distributed control strategy for a hybrid renewable nanogrid," *IEEE Trans. Ind. Electron.*, Vol. 53, No. 5, pp. 1453–1460, October 2006.

[17] Jin, C., Wang, P., Xiao, J., Tang, Y., and Choo, F. H., "Implementation of hierarchical control in DC microgrids," *IEEE Trans. Ind. Electron.*, Vol. 61, No. 8, pp. 4032–4042, August 2014.

[18] Kwasinski, A., and Onwuchekwa, C. N., "Dynamic behavior and stabilization of DC microgrids with instantaneous constant-power loads," *IEEE Trans. Power Electron.*, Vol. 26, No. 3, pp. 822–834, March 2011.

[19] Anand, S., Fernandes, B. G., and Guerrero, J., "Reduced order model and stability analysis of low voltage DC microgrid," *Ind. Electron. IEEE Trans.*, 2012.

[20] Shafiee, Q., Dragicevic, T., Vasquez, J. C., and Guerrero, J. M., "Modeling, stability analysis and active stabilization of multiple DC-microgrid clusters," *2014 IEEE International Energy Conference (ENERGYCON)*, pp. 1284–1290, May 2014.

[21] Vrana, T. K., Beerten, J., Belmans, R., and Fosso, O. B., "A classification of DC node voltage control methods for HVDC grids," pp. 137–144, 2013.

[22] Salomonsson, D., Söder, L., and Sannino, A., "Protection of low-voltage DC microgrids," *IEEE Trans. Power Deliv.*, Vol. 24, No. 3, pp. 1045–1053, July 2009.

[23] Corradini, L., Mattavelli, P., Tedeschi, E., and Trevisan, D., "High-bandwidth multisampled digitally controlled DC-DC converters using ripple compensation," *IEEE Trans. Ind. Electron.*, Vol. 55, pp. 1501–1508, 2008.

[24] Blasko, V., and Kaura, V., "A new mathematical model and control of a three-phase AC-DC voltage source converter," *IEEE Trans. Power Electron.*, Vol. 12, No. 1, pp. 116–123, January 1997.

APPENDIX A

Converter-Based Time Constant

V_{Nom}, V_{min}, C, and P_{rated} are the nominal voltage of system, the minimum voltage of the system, capacitance, and the rated power of the converter, respectively. The voltage ratio and the stored energy at the nominal and minimum voltages are shown below:

$$\begin{aligned} \alpha &= \frac{V_{\text{min}}}{V_{\text{Nom}}} \\ E_{\text{Nom}} &= C\frac{V_{Nom}^2}{2} \\ E_{\text{min}} &= C\frac{V_{\text{min}}^2}{2} \end{aligned} \tag{A1}$$

For a constant power, P_{rated}, drawn from the capacitor, τ is estimated using the following equation:

$$\begin{aligned} E_{\text{Nom}} - E_{\text{min}} &= \int_0^{\tau} P_{\text{rated}} dt \\ C\frac{V_{\text{Nom}}^2}{2} - C\frac{V_{\text{min}}^2}{2} &= \int_0^{\tau} P_{\text{rated}} dt \end{aligned} \tag{A2}$$

Replacing V_{min} by αV_{Nom} in Eq. (A2) and integrating the constant power over τ, τ is given as follows:

$$\tau = \frac{(1-\alpha^2)CV_{\text{Nom}}^2}{2P_{\text{rated}}} \tag{A3}$$

APPENDIX B

System-Based Time Constant

For a modular DC system where N represents the number of converters that are in the system, the time constant of a single converter is given by the following equation as derived in Appendix A where C_n and P_{rated_n} are terminal capacitance and rated power of the nth converter, respectively and α is the ratio of nominal to minimum voltage

$$\tau_n = \frac{(1-\alpha^2)C_n V_{\text{Nom}}^2}{2P_{\text{rated}_n}} \tag{B1}$$

The average time constant, τ_{ave}, of the entire system is the sum of individual converter divided by the number of converters as shown below:

$$\tau_{\text{ave}} = \frac{\sum_{n=1}^{N} \frac{(1-\alpha^2)V_{\text{Nom}}^2 C_n}{2P_{\text{rated}_n}}}{N} \tag{B2}$$

APPENDIX C

Prospective Short Circuit Current Derivation

The fault current equations in a basic DC grid shown in Figure 1 are presented in Eq. (C1) where $i(t)$, $i(t)_{con}$, and $i(t)_c$ are the fault current in the cable, the fault current from the converter, and the fault current from the terminal capacitor (C_s), respectively

$$\begin{aligned} i(t) &= i(t)_{\text{con}} + i(t)_c \\ i(t)_c &= C_s\frac{dV_c}{dt} \end{aligned} \tag{C1}$$

And the voltage equations are shown in Eq. (C2) where $v(t)_c$, L, and R_c are the terminal voltage of the source, sum of the decoupling inductance and cable inductance, and the cable resistances, respectively

$$\begin{aligned} v(t)_c &= L\frac{di(t)}{dt} + R_c i(t) \\ C_s\frac{dv(t)_c}{dt} &= C_s L\frac{di^2(t)}{dt^2} + C_s R_c\frac{di(t)}{dt} \end{aligned} \tag{C2}$$

In the first few μ, the main fault current contribution is from the capacitor. Therefore, the converter current, $i(t)_{con}$, is set the initial value, I_o. Replacing $v(t)_c$ in Eq. (C2) by the current equation from Eq. (C1), the differential equation for the fault current is

$$C_s L\frac{d^2 i(t)}{dt^2} + C_s R_c\frac{di(t)}{dt} - i(t) = -I_o \tag{C3}$$

Solving Eq. (C3), the fault current, $i(t)$, is

$$i(t) = \frac{I_o e^{-\frac{t\left(\frac{\sqrt{C_s R^2 - 4L}}{\sqrt{C_s}} + R\right)}{2L}} \left(\sqrt{C_s R^2 - 4L}\left(e^{\frac{t\sqrt{C_s R^2 - 4L}}{\sqrt{C_s}L}} + 1\right) + \sqrt{C_s}R\left(e^{\frac{t\sqrt{C_s R^2 - 4L}}{\sqrt{C_s}L}} - 1\right)\right)}{2\sqrt{C_s R^2 - 4L}} \tag{C4}$$

BIOGRAPHIES

Tsegay Gebremedhin Hailu received his M.Sc. degree in electrical engineering from Delft University of Technology, the Netherlands, in 2012, where he is currently working toward a Ph.D. degree. His current research focus is DC microgrids and DC distribution grids.

Laurens Mackay was born in Zeist, the Netherlands, and grew up close to Basel, Switzerland. He obtained his Bachelor and Master of Science in Electrical Engineering and Information Technology at the Swiss Federal Institute of Technology Zurich (ETH) in 2011 and 2012, respectively. He started working on DC distribution grids in his master's thesis. Since 2014, he is pursuing his PhD at Delft University of Technology, the Netherlands. His research interests are all aspects of DC distribution grids.

Laura M. Ramirez-Elizondo is an assistant professor at the DC Systems, Energy Conversion & Storage group. In 2003, she received her bachelor's degree in Electrical Engineering and her bachelor's degree in music with a major in piano at the Universidad de Costa Rica. She graduated with honors from her M.Sc. studies in Electrical Power Engineering at Delft University of Technology in 2007. She holds a PhD in electrical engineering from the Delft University of Technology (2013). Her research interests include power electronics and power systems.

Jan A. Ferreira received his B.Sc.Eng., M.Sc.Eng., and Ph.D. degrees in Electrical Engineering from the Rand Afrikaans University, Johannesburg, South Africa, in 1981, 1983, and 1988, respectively. In 1981, he was with the Institute of Power Electronics and Electric Drives, Technical University of Aachen, and worked in industry at ESD (Pty) Ltd from 1982 to 1985. From 1986, until 1997, he was at the Faculty of Engineering, Rand Afrikaans University, where he held the Carl and Emily Fuchs Chair of Power Electronics in later years. Since 1998, he is a professor at the Delft University of Technology in The Netherlands. Dr. Ferreira is a fellow of the IEEE. His research interests include power electronics and power systems.